CZECH TECHNICAL UNIVERSITY IN PRAGUE

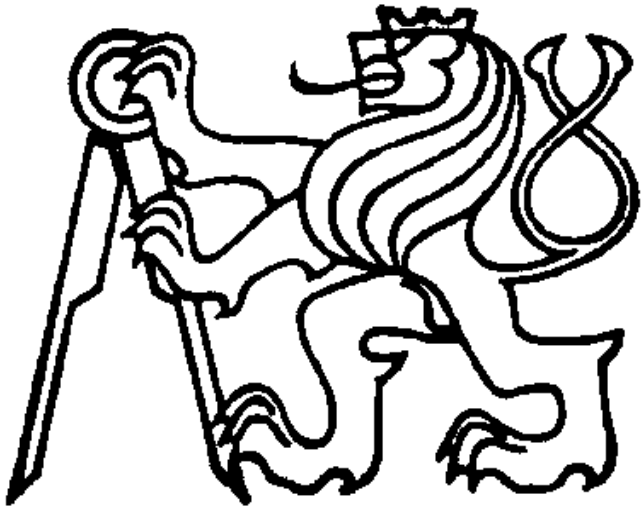

SUMMARY OF THE DISSERTATION THESIS

Czech Technical University in Prague
Faculty of Nuclear Sciences and Physical Engineering
Department of Mathematics

Radek Honzátko

NUMERICAL SIMULATIONS OF INCOMPRESSIBLE FLOWS WITH DYNAMICAL AND AEROELASTIC EFFECTS

Study Branch: Mathematical Engineering

Summary of the Ph.D. Thesis

Prague, August 2007

The dissertation thesis was elaborated during the doctoral study at the Department of Mathematics, Faculty of Nuclear Sciences and Physical Engineering (FNSPE), Czech Technical University in Prague (CTU).

Ph.D. candidate:	Ing. Radek Honzátko Department of Technical Mathematics Faculty of Mechanical Engineering, CTU in Prague Karlovo náměstí 13, 121 35 Praha 2 - Nové Město
Supervisor:	Prof. RNDr. Karel Kozel, DrSc. Department of Technical Mathematics Faculty of Mechanical Engineering, CTU in Prague Karlovo náměstí 13, 121 35 Praha 2 - Nové Město
Co-supervisor:	Ing. Jaromír Horáček, CSc. Institute of Thermomechanics AS CR Dolejškova 1402/5, 182 00 Praha 8
Opponents:	Prof. Ing. František Maršík, DrSc. Institute of Thermomechanics AS CR Dolejškova 5, 182 00 Praha 8
	Doc. Dr. Ing. Michal Beneš Department of Mathematics FNSPE CTU in Prague, Trojanova 13, 120 00 Praha 2

This abstract was issued on: .....

The defence of the dissertation thesis takes place on ..... in the room No. ....., FNSPE CTU in Prague, ...

The dissertation thesis is available in the Office for Research and Science of the FNSPE CTU in Prague, Břehová 7, 115 19 Praha 1.

Prof. Ing. Miloslav Havlíček, DrSc.
Chair of the Committee
FNSPE CTU in Prague, Trojanova 13, 120 00 Praha 2

State of the Art

The interaction of fluid flow and an elastic structure plays an important role in many technical disciplines, such as aircraft industry (e. g. wing deformations), mechanical engineering (flows around turbomachinery blades, compressor blades, in flexible pipes), civil engineering (stability of bridges), nuclear engineering (flows about fuel elements, heat exchanger vanes), etc. The impact of aeroelasticity on stability and control (flight mechanics) has increased substantially in recent years. Most aeroelastic phenomena are of an undesirable character, leading to loss of design effectiveness or even structural failure as in the case of aircraft wing flutter. The research in aeroelasticity or hydroelasticity focuses on the interaction between moving fluids and vibrating structures. Widely used commercial codes, e. g. NASTRAN, FLUENT or ANSYS, can only solve particular problems of aeroelasticity and hydroelasticity and are mainly limited to linearized models. The modelling of post-flutter behaviour, limit-cycle oscillations and other nonlinear phenomena for large amplitudes of vibration began to be more important. Flutter at large deformations can be studied by analytical methods only in some special cases. Thus, numerical simulations of nonlinear behaviour of dynamical systems become more important, since they allow to consider changes of the flow domain in time, nonlinear behaviour of the elastic structure, to solve simultaneously the evolution system for the fluid flow and for the oscillating structure, etc.

An up-to-date extensive book related to the aeroelasticity topics is, e. g., [1]. It provides insight into the fundamentals of classical linear aeroelasticity and also describes recent results on the research dealing with nonlinear aeroelasticity as well as major advances in the modelling of unsteady aerodynamic flows using methods of computational fluid dynamics. Further modern books concerning fluid-structure interactions are, e. g., [2, 3].

Research Goals

The main goal of this work is to develop and implement numerical methods for solving incompressible flows with aeroelastic effects. The emphasis is placed on numerical simulations of flow induced vibrations of a profile. The effort is aimed for numerical solution of two-dimensional inviscid incompressible flows and eventual extension of the developed methods for viscous laminar flows. Further objectives are to validate the methods against experimental

and theoretical data and to present numerical results of realistic engineering problems demonstrating the implemented solver applicability.

Methods Used

Finite volume method is applied to the spatial discretization of the implemented two-dimensional numerical model. Several standard explicit numerical schemes, such as Lax-Wendroff scheme or Runge-Kutta scheme, are used together with artificial compressibility method for numerical solution of steady state flows. An artificial dissipation term is added for the sake of stability. For simulations of unsteady flows, either the explicit Lax-Wendroff scheme in conjunction with artificial compressibility approach or a dual-time stepping scheme are employed. In the latter case, the physical time is treated implicitly whereas explicit discretization is applied to the dual (also called artificial, pseudo or iterative) time. Since aeroelastic effects are considered, there is generally a change of a solution domain in time. Small disturbance theory and arbitrary Lagrangian-Eulerian method are used to cope with this issue. System of two ordinary differential equations representing governing equations of the profile motion with two degrees of freedom is solved numerically by the fourth-order Runge-Kutta method.

Research Results

In this thesis, numerical results of steady state flows over a profile and unsteady flows concerning flow induced vibrations of the profile are presented. The stress is laid on results of inviscid incompressible flows. In order to validate developed techniques, numerical solutions are compared with experimental and theoretical data. Good agreement can be observed. For all steady state calculations, two numerical schemes are used and their solutions presented and compared respectively. In the case of unsteady flows, results of two different approaches for solving unsteady governing equations are shown and also mutually compared. Preliminary results of laminar viscous flows are presented.

Contents

Introduction **1**

1 Mathematical Models **2**

2 Numerical Solution of Steady State Flows **4**

3 Numerical Solution of Unsteady Flows **5**

4 Numerical Realization of Boundary Conditions **8**

5 Governing Equations of the Profile Motion **9**

6 Mesh Generation and Mesh Movement Description **10**

7 Numerical Results **11**
7.1 Steady State Solutions 11
7.2 Prescribed Profile Oscillation 12
7.3 Two Degrees of Freedom System 14
7.4 Viscous Flow Simulations 17

Conclusions **18**

Anotace **20**

Introduction

Aeroelasticity is the science which studies the interaction among inertial, elastic, and aerodynamic forces. Aeroelastic phenomena play an important role in many technical disciplines, such as aircraft industry (e. g. wing deformations), mechanical engineering (flows around turbomachinery blades, compressor blades, in flexible pipes), civil engineering (stability of bridges), nuclear engineering (flows about fuel elements, heat exchanger vanes), etc. Most of them are of an undesirable character, leading to loss of design effectiveness or even structural failure as in the case of aircraft wing flutter or the Tacoma Narrows Bridge disaster.

The research in aeroelasticity or hydroelasticity focuses on the interaction between moving fluids and vibrating structures. Problems involving a permanent flow about a vibrating structure are referred to as flow induced vibration problems. Recently, the attention has been focused on nonlinear behaviour of such dynamical systems, for instance on the existence and stability of limit-cycle motions or post-flutter behaviour.

Widely used commercial codes, e. g. NASTRAN, FLUENT or ANSYS, can only solve particular problems of aeroelasticity and hydroelasticity and are mainly limited to linearized models. However, the modelling of nonlinear phenomena for large amplitudes of vibration and numerical simulations of nonlinear behaviour of dynamical systems began to be more important.

This thesis deals with a numerical simulation of flow induced vibrations of a profile with generally two degrees of freedom. The first part is devoted to systems of Euler and Navier-Stokes equations representing mathematical models of two-dimensional inviscid and viscous incompressible flows, and boundary conditions employed at boundaries of solution domains considered in this work. Since non-dimensional forms of the mentioned mathematical models are used in numerical simulations performed, the transformation from dimensional to non-dimensional form is also carried out in this part.

The second part deals with numerical methods applied to numerical simulations. It briefly summarizes the finite volume method, introduces artificial compressibility method used for solving steady state inviscid and viscous incompressible flows and presents explicit numerical schemes implemented by the author. Stability analysis for scalar linear advection equation with constant coefficients in two space dimensions is also carried out. It results in a time step restriction exploited in a slightly changed form in implemented algorithms. Further, two numerical methods for solving unsteady incompressible flows are presented, namely artificial compressibility approach and

dual-time stepping method. Two methods for treating domain deformations due to the profile motion are introduced, particularly small disturbance theory and arbitrary Lagrangian-Eulerian method. Numerical schemes employed in unsteady numerical simulations are described in detail. All used boundary conditions for both inviscid and viscous flow simulations are discussed. In the case of slip wall boundary condition, four different ways of computing a pressure at the wall are explained and their influence on a solution compared respectively. Two cases of profile motion are considered, prescribed oscillation around an elastic axis and flow induced profile vibrations with two degrees of freedom. Governing equations of profile motion are derived and their numerical realization is explained.

The third part presents numerical results achieved within this work. Results of inviscid flows and also rather preliminary results of laminar viscous flows are presented. The emphasis is placed on inviscid flow simulations. Numerical solutions of both steady state flows and unsteady flows are shown. They are compared with experimental and theoretical data.

1 Mathematical Models

Formally speaking, incompressible flows are those for which the density is constant on particle paths. If all the particles of interest originate in a region of uniform density, then the density remains uniform. In this work, the incompressibility assumption is related to a uniform constant density in a domain of interest. Then, the equation of state is $\rho =$ constant (at constant temperature).

The behaviour of two-dimensional incompressible viscous flows with constant viscosity is described by the system of Navier-Stokes equations written in conservative non-dimensional vector form:

$$(\mathbb{D}\mathsf{W})_{\mathsf{t}} + \mathsf{F}^c_{\mathsf{x}} + \mathsf{G}^c_{\mathsf{y}} = \frac{1}{Re}\left(\mathsf{F}^v_{\mathsf{x}} + \mathsf{G}^v_{\mathsf{y}}\right), \tag{1}$$

$$\mathsf{W} = \begin{pmatrix} \mathsf{p} \\ \mathsf{u} \\ \mathsf{v} \end{pmatrix}, \ \mathsf{F}^c = \begin{pmatrix} \mathsf{u} \\ \mathsf{u}^2 + \mathsf{p} \\ \mathsf{uv} \end{pmatrix}, \ \mathsf{G}^c = \begin{pmatrix} \mathsf{v} \\ \mathsf{uv} \\ \mathsf{v}^2 + \mathsf{p} \end{pmatrix}, \tag{2}$$

$$\mathsf{F}^v = \begin{pmatrix} 0 \\ \mathsf{u}_{\mathsf{x}} \\ \mathsf{v}_{\mathsf{x}} \end{pmatrix}, \ \mathsf{G}^v = \begin{pmatrix} 0 \\ \mathsf{u}_{\mathsf{y}} \\ \mathsf{v}_{\mathsf{y}} \end{pmatrix}, \tag{3}$$

with

$$\mathbb{D} = \begin{pmatrix} 0 & 0 & 0 \\ 0 & 1 & 0 \\ 0 & 0 & 1 \end{pmatrix}. \tag{4}$$

Instead of (3) it is sometimes preferred to use viscous fluxes in the form:

$$\mathsf{F}^v = \begin{pmatrix} 0 \\ 2\mathsf{u}_\mathsf{x} - \frac{2}{3}(\mathsf{u}_\mathsf{x} + \mathsf{v}_\mathsf{y}) \\ \mathsf{u}_\mathsf{y} + \mathsf{v}_\mathsf{x} \end{pmatrix}, \; \mathsf{G}^v = \begin{pmatrix} 0 \\ \mathsf{u}_\mathsf{y} + \mathsf{v}_\mathsf{x} \\ 2\mathsf{v}_\mathsf{y} - \frac{2}{3}(\mathsf{u}_\mathsf{x} + \mathsf{v}_\mathsf{y}) \end{pmatrix}. \tag{5}$$

They are equivalent to (3), since the solution satisfies the continuity equation $\mathsf{u}_\mathsf{x} + \mathsf{v}_\mathsf{y} = 0$.

Here, p is pressure, u, v are velocity vector components and Re designates Reynolds number. Indices t, x, y denote partial derivatives of corresponding variables with respect to time and spatial coordinates, respectively. The vector W is called the vector of conservative variables, $\mathsf{F}^c \equiv \mathsf{F}^c(\mathsf{W})$, $\mathsf{G}^c \equiv \mathsf{G}^c(\mathsf{W})$ are convective fluxes and F^v, G^v are viscous fluxes.

If the viscosity is neglected (i. e. $Re \to \infty$) in the Navier-Stokes equations (1), the Euler equations for two-dimensional inviscid incompressible flows are obtained. The non-dimensional vector form of this system is

$$(\mathbb{D}\mathsf{W})_\mathsf{t} + \mathsf{F}^c_\mathsf{x} + \mathsf{G}^c_\mathsf{y} = 0, \tag{6}$$

$$\mathsf{W} = \begin{pmatrix} \mathsf{p} \\ \mathsf{u} \\ \mathsf{v} \end{pmatrix}, \; \mathsf{F}^c = \begin{pmatrix} \mathsf{u} \\ \mathsf{u}^2 + \mathsf{p} \\ \mathsf{uv} \end{pmatrix}, \; \mathsf{G}^c = \begin{pmatrix} \mathsf{v} \\ \mathsf{uv} \\ \mathsf{v}^2 + \mathsf{p} \end{pmatrix}, \tag{7}$$

with

$$\mathbb{D} = \begin{pmatrix} 0 & 0 & 0 \\ 0 & 1 & 0 \\ 0 & 0 & 1 \end{pmatrix}. \tag{8}$$

When governing equations are the Navier-Stokes equations (1)-(4), the inlet, outlet and non-slip wall boundary conditions are taken into account. When the mathematical model is represented by the system of Euler equations (6)-(8), the inlet, outlet and slip wall boundary conditions are considered.

2 Numerical Solution of Steady State Flows

The finite volume method is used as a discretization method. Let us consider a system of conservation laws written in a vector form:

$$\mathsf{W}_{\mathsf{t}} + \nabla \cdot \mathsf{F}(\mathsf{W}) = 0\,. \tag{9}$$

This system can be used for numerical simulations of both steady state flows (time marching method) or unsteady flows. Here $\mathsf{W} : \mathbb{R}^r \to \mathbb{R}^s$, $\mathsf{W} = (w_1, \ldots, w_s)$ is an s-dimensional vector of conserved quantities and $\mathsf{F}(\mathsf{W}) = (\mathsf{F}_1(\mathsf{W}), \ldots, \mathsf{F}_r(\mathsf{W}))$ is called flux. Symbol $\nabla\cdot$ designates a divergence operator, where $\nabla = \left(\frac{\partial}{\partial \mathsf{x}_1}, \ldots, \frac{\partial}{\partial \mathsf{x}_r}\right)$ and $\mathsf{x}_1, \ldots, \mathsf{x}_r$ are spatial coordinates of $\mathbb{R}^r$. A finite volume scheme can be defined as follows

$$\left(\mathsf{W}_i^{n+1} - \mathsf{W}_i^n\right)|C_i| + \Delta\mathsf{t} \sum_{j \in N_i} H_{ij}^* |E_{ij}| = 0\ . \tag{10}$$

Here, $\Delta\mathsf{t} = \mathsf{t}^{n+1} - \mathsf{t}^n$, the superscript n denotes a time level, N_i is an index set involving indices of all neighbouring cells of the cell C_i, $|C_i|$ stands for a volume of the cell C_i, $|E_{ij}|$ is the length of the edge E_{ij} between the cell C_i and a neighbouring cell C_j and

$$H_{ij}^* \approx \frac{1}{\Delta\mathsf{t}|E_{ij}|} \int_{\mathsf{t}^n}^{\mathsf{t}^{n+1}} \int_{E_{ij}} \mathsf{F}\left(\mathsf{W}(\mathsf{x}_1, \ldots, \mathsf{x}_r, \mathsf{t})\right) \cdot \mathbf{n}_{ij}\, dl\, d\mathsf{t} \tag{11}$$

is called the 'numerical flux'. The superscript $*$ stands for a time instant at which the numerical flux is evaluated. For instance, $* \equiv n$ represents time t^n and (10) results in an explicit numerical scheme. The symbol $\mathbf{n}_{ij}$ denotes an outward-pointing unit normal to the edge E_{ij} (i. e. normal vector to the edge E_{ij} pointing out from the cell C_i and into the neighbouring cell C_j). In this work, mathematical models of three equations for two-dimensional problems are considered. Hence, $s = 3$ and $r = 2$. Spatial coordinates are usually denoted x, y instead of $\mathsf{x}_1, \mathsf{y}_2$.

The method of artificial compressibility is employed for numerical solution of steady state incompressible flows. The principle of the method consists in modifying the governing equations by the introduction of the time derivative of pressure to the continuity equation. It is represented by a corresponding change of matrix $\mathbb{D}$ in (1) or (6) as follows:

$$\mathbb{D}_\beta = \begin{pmatrix} \frac{1}{\beta^2} & 0 & 0 \\ 0 & 1 & 0 \\ 0 & 0 & 1 \end{pmatrix}, \tag{12}$$

where $\beta \in \mathbb{R}^+$ is a coefficient. Since this method is used to obtain an asymptotic steady solution, the variable t acts for an auxiliary variable which allows using marching procedures to solve (1)-(3) or (6)-(7) with (12). If the solution of (1)-(3), resp. (6)-(7) with (12) converges to a steady solution, i. e. one independent of t, then this solution is a steady solution of (1)-(4), resp. (6)-(8).

For numerical simulations of both viscous and inviscid steady state flows, Lax-Wendroff scheme in Richtmyer form, MacCormack form or a multistage Runge-Kutta scheme is employed. All schemes are implemented in a cell-centered form, i. e. the average values of conservative variables are stored in centres of gravity of finite volume cells. An artificial dissipation term is added to the schemes to ensure their stability.

Since all numerical schemes used are explicit schemes, they are conditionally stable, i. e. the time step has to be limited. In this work, the expression

$$\Delta \mathsf{t} = \min_{C_i,\, j} \frac{|C_i|\,\mathrm{CFL}}{\rho(\mathbb{A})\,|\Delta \mathsf{y}_{ij}| + \rho(\mathbb{B})\,|\Delta \mathsf{x}_{ij}|},\ i \in I,\ j \in N_i \tag{13}$$

is used for inviscid flow simulations. Here, I is an index set of indices of all cells discretizing the computational domain, $\rho(\mathbb{A})$ and $\rho(\mathbb{B})$ are spectral radii of Jacobi matrices of convective fluxes in x-direction and y-direction, respectively and CFL is called Courant number. As far as Navier-Stokes equations is concerned, the relation

$$\Delta \mathsf{t} = \min_{C_i,\, j} \frac{|C_i|^2\,\mathrm{CFL}}{\rho(\mathbb{A})|C_i|\,|\Delta \mathsf{y}_{ij}| + \rho(\mathbb{B})|C_i|\,|\Delta \mathsf{x}_{ij}| + \frac{2}{Re}\left(\Delta \mathsf{y}_{ij}^2 + \Delta \mathsf{x}_{ij}^2\right)},. \tag{14}$$

$i \in I$, $j \in N_i$ is considered. For both the Lax-Wendroff scheme in Richtmyer form and the Lax-Wendroff scheme in MacCormack form it holds $\mathrm{CFL} = 1$. For the four-stage Runge-Kutta scheme with coefficients $\alpha_1 = \frac{1}{4}$, $\alpha_2 = \frac{1}{3}$, $\alpha_3 = \frac{1}{2}$, $\alpha_4 = 1$ the value of this number is $\mathrm{CFL} = 2\sqrt{2}$.

Ideally, the stationary residuum descends to the machine zero provided that the numerical solution converges to the steady state one. The global behaviour of the solution during the time-marching process is followed by the L_2 norm of the stationary residuum.

3 Numerical Solution of Unsteady Flows

This section deals with a numerical solution of incompressible flows over a vibrating profile. Two degrees of freedom of the profile are generally consid-

ered. It can oscillate around an elastic axis and in the vertical direction.

If the profile is only allowed to rotate around the elastic axis with small amplitudes, the method called 'small disturbance theory' can be used to handle the profile motion. It allows to approximate the rotation of an inviscid wall around a fixed point by the rotation of a normal vector to the wall. It can only be used under the assumption of a sufficiently small angle of the rotation. In this work, this method is employed to handle the rotation of a profile around an elastic axis (one degree of freedom) with the maximal admissible angle of attack $|\varphi| \leq 6°$. There is no real movement of the profile with the use of this approach and therefore the grid is fixed, which saves computational time.

On the other hand, when the motion of the profile is more complex (e. g. two degrees of freedom) or with large amplitudes, consequently rising deformations of the computational domain are treated using so called arbitrary Lagrangian-Eulerian (ALE) method. It is based on an ALE mapping

$$\mathcal{A}_{\mathsf{t}} : \Omega_{\text{ref}} \to \Omega_{\mathsf{t}}\,, \quad \xi \in \Omega_{\text{ref}} \to X = X(\xi, \mathsf{t}) = \mathcal{A}_{\mathsf{t}}(\xi) \in \Omega_{\mathsf{t}} \tag{15}$$

of the reference configuration $\Omega_{\text{ref}} \equiv \Omega_0$ at time $\mathsf{t} = 0$ onto the current configuration Ω_{t} at time $\mathsf{t} \in T$ (see Figure 1). The governing integral equation

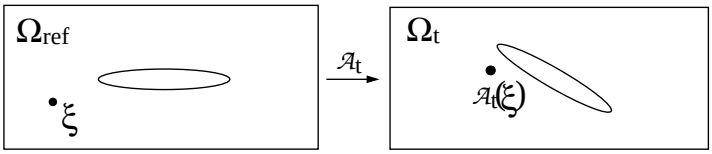

Figure 1: ALE mapping of the reference configuration $\Omega_{\text{ref}} \equiv \Omega_0$ onto the current configuration Ω_{t}.

for inviscid flow is

$$\frac{d}{d\mathsf{t}} \int_{C_i(\mathsf{t})} \mathbb{D}\mathsf{W}\, d\Omega_X + \oint_{\partial C_i(\mathsf{t})} \left(\tilde{\mathsf{F}}^c(\mathsf{W}, w_1)\, d\mathsf{y} - \tilde{\mathsf{G}}^c(\mathsf{W}, w_2)\, d\mathsf{x} \right) = 0\,, \tag{16}$$

where $\tilde{\mathsf{F}}^c(\mathsf{W}, w_1) = \mathsf{F}^c(\mathsf{W}) - w_1 \mathbb{D}\mathsf{W}$ and $\tilde{\mathsf{G}}^c(\mathsf{W}, w_2) = \mathsf{G}^c(\mathsf{W}) - w_2 \mathbb{D}\mathsf{W}$, whereas $(w_1, w_2)^T$ is the grid velocity vector. Similarly, for viscous flow the integral

form of the Navier-Stokes equations in ALE formulation reads

$$\frac{d}{d\mathsf{t}}\int_{C_i(\mathsf{t})}\mathbb{D}\mathsf{W}\,d\Omega_X + \tag{17}$$
$$+\oint_{\partial C_i(\mathsf{t})}\left[\left(\tilde{\mathsf{F}}^c(\mathsf{W},w_1)-\frac{1}{Re}\mathsf{F}^v\right)d\mathsf{y}-\left(\tilde{\mathsf{G}}^c(\mathsf{W},w_2)-\frac{1}{Re}\mathsf{G}^v\right)d\mathsf{x}\right]=0\,.$$

When the artificial compressibility method is used, the matrix $\mathbb{D}$ is substituted by the matrix $\mathbb{D}_\beta$ (see Eq. (12)). It is desirable that this solution method predicts exactly a uniform flow because it is then mathematically consistent. This requirement is satisfied only when the numerical scheme chosen for solving the flow problem, and the algorithm constructed for updating the dynamic mesh, satisfy a discrete Geometric Conservation Law (GCL). It is defined by

$$|C_i(\mathsf{t}^{n+1})|-|C_i(\mathsf{t}^n)|=\int_{\mathsf{t}^n}^{\mathsf{t}^{n+1}}\oint_{\partial C_i(X,\mathsf{t})}(w_1\,d\mathsf{y}-w_2\,d\mathsf{x})\,d\mathsf{t}, \tag{18}$$

where $\partial C_i(X,\mathsf{t})$ denotes a boundary of the cell C_i. It states that the change in area of each cell between t^n and t^{n+1} must be equal to the area swept by the cell boundary during $\Delta\mathsf{t}=\mathsf{t}^{n+1}-\mathsf{t}^n$.

Two approaches are used for numerical solution of unsteady governing equations. First, an artificial compressibility approach is applied. The principle of this method lies in changing the mathematical models of incompressible flows in a way, which directly allows to use time-marching procedures. Governing equations are modified by adding an unsteady term to the continuity equation in the same way as for the artificial compressibility method used for steady state simulations. The parameter β has to be a big positive number. On the other hand, to keep a reasonable length of the time step , β has to be bounded from above. Numerical calculations show, that $\beta=10$ is a proper choice. However, the unsteady numerical solution can be altered by this change with respect to the numerical solution of the original mathematical models.

Therefore, a dual-time stepping method is employed. Unlike the artificial compressibility approach, it provides a possibility to develop a time-accurate time-marching scheme for unsteady incompressible flows. This approach requires the addition of derivatives of a fictious dual time τ to each of the three equations to give

$$\mathbb{D}_\beta\mathsf{W}_\tau+\mathbb{D}\mathsf{W}_\mathsf{t}+\mathsf{F}^c_\mathsf{x}+\mathsf{G}^c_\mathsf{y}=\frac{1}{Re}\left(\mathsf{F}^v_\mathsf{x}+\mathsf{G}^v_\mathsf{y}\right) \tag{19}$$

for viscous flows and

$$\mathbb{D}_\beta \mathsf{W}_\tau + \mathbb{D}\mathsf{W}_\mathsf{t} + \mathsf{F}^c_\mathsf{x} + \mathsf{G}^c_\mathsf{y} = 0 \tag{20}$$

for inviscid flows. A steady state solution in dual time ($\partial\mathsf{p}/\partial\tau$, $\partial\mathsf{u}/\partial\tau$, $\partial\mathsf{v}/\partial\tau \to 0$) corresponds to an instantaneous unsteady solution in real time t. Both the equations (19) and (20) can be rewritten in a compact form as:

$$\mathsf{W}_\tau + \mathbb{D}\mathsf{W}_\mathsf{t} + R(\mathsf{W}) = 0, \tag{21}$$

where $R(\mathsf{W})$ is the steady residuum comprising also the parameter β. If derivatives with respect to the real time t are discretized using a three-point backward formula, it results in an implicit scheme

$$\mathsf{W}_\tau = -\frac{3\mathsf{W}^{n+1} - 4\mathsf{W}^n + \mathsf{W}^{n-1}}{2\Delta\mathsf{t}} - R\left(\mathsf{W}^{n+1}\right) \equiv -\tilde{R}\left(\mathsf{W}^{n+1}\right), \tag{22}$$

which is second-order accurate in time. Here, $\tilde{R}\left(\mathsf{W}^{n+1}\right)$ is called unsteady residuum. The superscript n is associated with the real time. The required real-time accurate solution at time level $n+1$ satisfies $\tilde{R}\left(\mathsf{W}^{n+1}\right) = 0$ and this is found by marching Eq. (22) to a steady state in dual time. The dual-time derivative is treated explicitly using a four-stage Runge-Kutta scheme in this work.

4 Numerical Realization of Boundary Conditions

The boundary of a computational domain is approximated by a piecewise linear curve. Its linear segments are represented by edges of finite volume cells discretizing the computational domain and adjoining the boundary. There are introduced ghost cells lying out of the computational domain and adjoining the boundary. They are constructed by reflection of an interior finite volume cell adjacent to the boundary with respect to the edge on the boundary as shown in Figure 2. These ghost cells are employed in the numerical realization of boundary conditions. Having the vector of conservative variables in an interior cell adjacent to the boundary and in a corresponding ghost cell, standard algorithms used for finite volume schemes can be applied to boundary faces in the same manner as to interior faces of the computational domain.

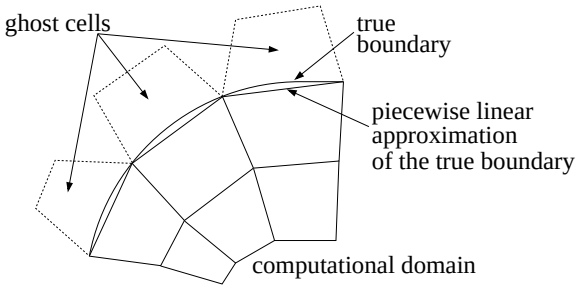

Figure 2: Ghost cells and piecewise linear approximation of the true boundary.

5 Governing Equations of the Profile Motion

Two cases of a profile motion are considered. Note that the governing equations of motion will be considered in dimensional variables. First, the profile can only rotate around a fixed point called the elastic axis with a prescribed change of an angle of attack in time. The prescribed oscillation of the profile is driven by the formula:

$$\varphi = \varphi_0 \sin\left(2\pi f t + \varphi_{\text{init}}\right), \tag{23}$$

where φ [rad] is the angle of rotation of the profile measured from the position of equilibrium, φ_0 [rad] is the amplitude of oscillations, f [Hz] is the frequency of oscillations, φ_{init} [rad] is an initial phase and t [s] is time. For a positive angle of attack φ the profile is rotated in the clockwise direction.

Second, it is assumed that the profile is freely vibrating with two degrees of freedom. It means, that it is taken as a solid body which can oscillate in the vertical direction and in the angular direction around the elastic axis. After including terms of proportional damping the governing equations of motion have the form

$$\begin{aligned} m\ddot{h} + S_\varphi \ddot{\varphi}\cos\varphi - S_\varphi \dot{\varphi}^2 \sin\varphi + k_{hh} h + d_{hh}\dot{h} &= -L(t), \\ S_\varphi \ddot{h}\cos\varphi + I_\varphi \ddot{\varphi} + k_{\varphi\varphi}\varphi + d_{\varphi\varphi}\dot{\varphi} &= M(t). \end{aligned} \tag{24}$$

Here, m [kg] is the mass of the profile, S_φ [kg m] is the static momentum around the elastic axis, I_φ [kg m^2] is the inertia moment around the elastic axis, k_{hh} [N m] denotes bending stiffness, $k_{\varphi\varphi}$ [N m/rad] is the torsional

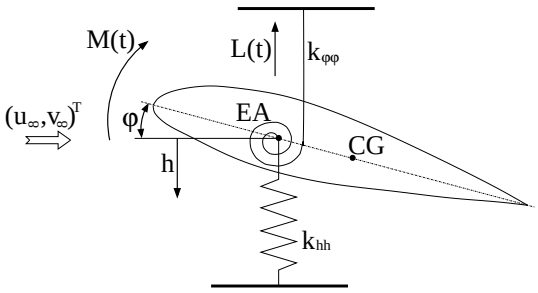

Figure 3: The elastic support of the profile on translational and rotational springs.

stiffness of the supporting springs, $L(t)$ [N] stands for the lift force acting in the vertical direction (upwards positive) and $M(t)$ [N m] is the torsional moment (clockwise positive). The coefficients of the proportional damping are considered in the form $d_{hh} = \varepsilon k_{hh}$ and $d_{\varphi\varphi} = \varepsilon k_{\varphi\varphi}$, where $\varepsilon \in \mathbb{R}$ is a small parameter. For small values of the angle φ and of its derivative $\dot{\varphi}$ (i. e. $\sin\varphi \approx \varphi$, $\cos\varphi \approx 1$, $\dot{\varphi}\varphi \approx 0$), Eqs. (24) transform to the well known linearized system

$$\begin{aligned} m\ddot{h} + S_\varphi\ddot{\varphi} + k_{hh}h + d_{hh}\dot{h} &= -L(t), \\ S_\varphi\ddot{h} + I_\varphi\ddot{\varphi} + k_{\varphi\varphi}\varphi + d_{\varphi\varphi}\dot{\varphi} &= M(t). \end{aligned} \tag{25}$$

The system (24) or (25) is completed with the initial conditions prescribing values $h(0)$, $\varphi(0)$, $\dot{h}(0)$, $\dot{\varphi}(0)$. The governing equations are transformed to the system of first-order ordinary differential equations and solved numerically by the fourth-order Runge-Kutta method.

6 Mesh Generation and Mesh Movement Description

Numerical simulations of flow past a profile in free space or placed in a channel are performed. Particularly, the profile NACA 0012 is used. It has a blunt leading edge and a sharp trailing edge. Therefore, a quadrilateral C-type mesh is the proper topology of boundary-conforming grid for considered

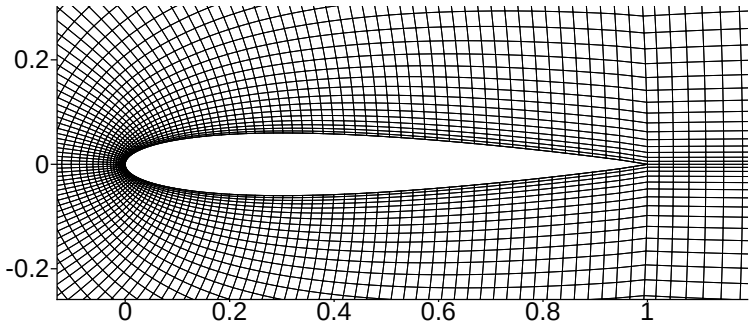

Figure 4: C-type mesh in a channel with the profile NACA 0012, detail near the profile, 135 points on the profile surface.

computational domain geometries. To this purpose, a Matlab script for generating these type of meshes for both the viscous and inviscid flow calculations was developed by the author. The detail of the C-type mesh near the profile is presented in Figure 4. When boundaries of a computational domain are moving the mesh moves in a given corresponding manner.

7 Numerical Results

7.1 Steady State Solutions

Several numerical results of steady state solutions of inviscid incompressible flow are presented and compared with experimental data. Numerical simulations of the external flow field around the profile NACA 0012 were performed. The geometry and dimensions of the computational domain are depicted in Figure 5. The quadrilateral structured C-type mesh with 121 point on the profile surface and 6720 cells in the solution domain was used.

Figure 6 presents the comparison of numerical data computed with the use of the Lax-Wendroff scheme in Richtmyer form (LWR scheme) and four-stage Runge-Kutta scheme (RK scheme) with experimental data. The profile is fixed in the zero angle of attack. The non-dimensional upstream velocity vector is $(\mathsf{u}_\infty, \mathsf{v}_\infty)^T = (1.0, 0.0)^T$ and the prescribed non-dimensional downstream pressure is $\mathsf{p}_{\text{out}} = 1.0$. Figure 6(a) compares the distribution of the non-dimensional velocity value squared $Q^2 = \mathsf{u}^2 + \mathsf{v}^2$ along the profile surface

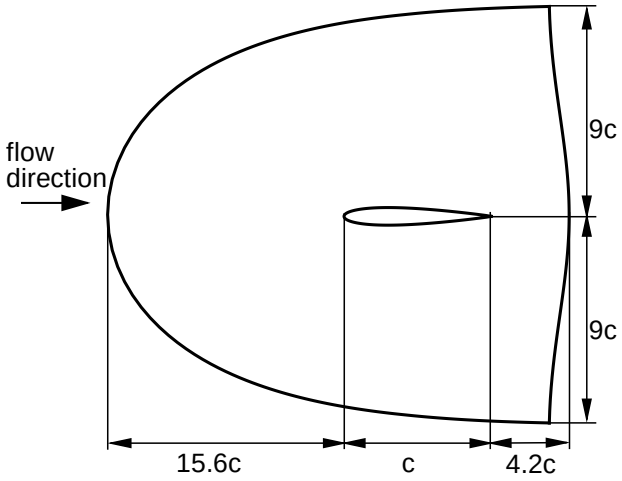

Figure 5: Solution domain used for numerical simulations of external aerodynamics.

in dependence on the length of the chord measured from the leading edge. The computed data are compared with experimental data of Luchta [4]. Figure 6(b) shows the comparison of the pressure coefficient distribution c_p along the profile surface in dependence on the length of the chord measured from the leading edge. Numerical data are compared with experimental data of Benetka [5, 6]. The computed values of the pressure and velocity along the profile surface are in a good agreement with the experimental values.

7.2 Prescribed Profile Oscillation

Results of numerical simulations of inviscid incompressible flow over the vibrating profile NACA 0012 in a channel are presented. The profile motion is driven by the formula (23) with $\varphi_0 = 3°$, $f = 30$ Hz and $\varphi_{\text{init}} = 0$. The position of the elastic axis EA measured along the chord from the leading edge of the profile is $\left(x^{\text{EA}}, y^{\text{EA}}\right)^T = (0.25c, 0.0)^T$, where the chord length is $c = 0.1322$ m. The upstream velocity is $(u_\infty, v_\infty)^T = (136.0, 0.0)^T$ m/s. The geometry of the channel and its proportions are sketched out in Figure 7.

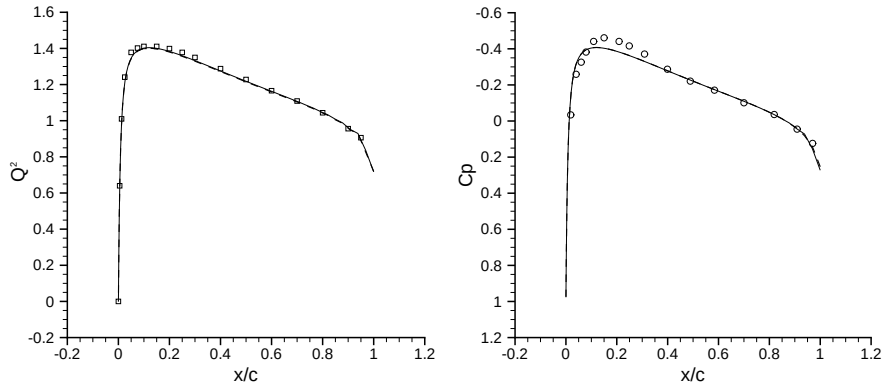

(a) The velocity value squared Q^2.

(b) The mean value of the pressure coefficient c_p.

Figure 6: (a) The velocity value squared Q^2 and (b) the mean value of the pressure coefficient c_p: ——, computed values (RK scheme); – – –, computed values (LWR scheme); □, Luchta experiment; ○, Benetka experiment.

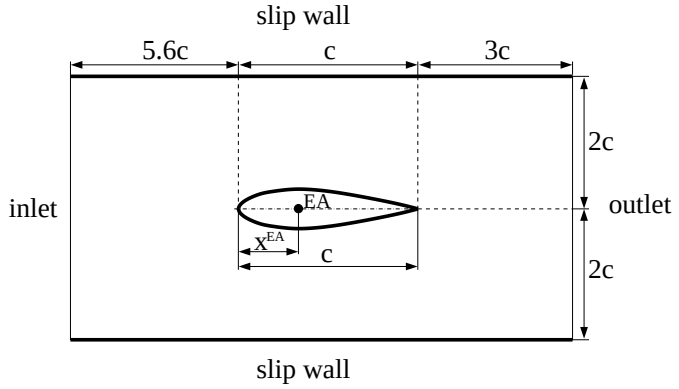

Figure 7: Channel geometry and its proportions.

In Figure 8, the distribution of the mean value of the pressure coefficient c_p, its real part c_p' and imaginary part c_p'' on the profile surface in dependence on the length of the chord measured from the leading edge is presented. The data are scaled to the pitching oscillation amplitude one radian and the upstream Mach number Ma = 0.4. The numerical results of the Lax-Wendroff scheme in Richtmyer form (LWR) with the use of the small disturbance theory (SDT) for the profile motion approximation, the LWR scheme in the ALE formulation and the numerical scheme in the ALE formulation using the dual-time stepping method (DTSM) are compared with the experimental and theoretical data of Triebstein [7] and experimental data of Benetka [8]. Concerning the LWR scheme, the artificial compressibility approach is applied. The parameter β considered in this approach was set to 10. All the mathematical approaches give practically identical values of the c_p coefficient. However, the computed values are somehow systematically shifted in the leading part of the profile probably due to neglecting the fluid compressibility. All computed results for real and imaginary part of the pressure coefficient have similar trends comparing to the Triebstein [7] and Benetka [8] data. The best fitting was obtained for the DTSM scheme and ALE method. The LWR scheme with the SDT approach seems to be the worst variant of the simulation.

Figure 9 shows isolines of pressure coefficient around the vibrating profile. The data are computed using the DTSM scheme in the ALE formulation. The isolines are plotted for the profile angles of attack $\varphi = 0°, \pm 3°$ during one period of oscillations. Note that when the profile moves opposite way (see figures (c) and (e)) the pressure filed around the profile is reflected.

7.3 Two Degrees of Freedom System

Numerical results of flow induced vibrations of the profile NACA 0012 with two degrees of freedom are presented. The flow is taken for inviscid incompressible. The solution domain is shown in Figure 5. The profile motion is described either by the system of two nonlinear ordinary differential equations of second order (24) or its linearized form (25). The following input quantities are used: $m = 0.086622$ kg, $S_\varphi = -0.000779673$ kg m, $I_\varphi = 0.000487291$ kg m^2, $k_{hh} = 105.109$ N/m, $k_{\varphi\varphi} = 3.695582$ N m/rad, $\varepsilon = 0.001$, $d = 0.05$ m, $c = 0.3$ m, $\rho = 1.225$ kg/m^3. The position of the elastic axis EA measured along the chord from the leading edge of the profile is $\left(x^{\mathrm{EA}}, y^{\mathrm{EA}}\right)^T = (0.4c, 0.0)^T$. The far-field flow velocity is considered in the range $5 - 45$ m/s.

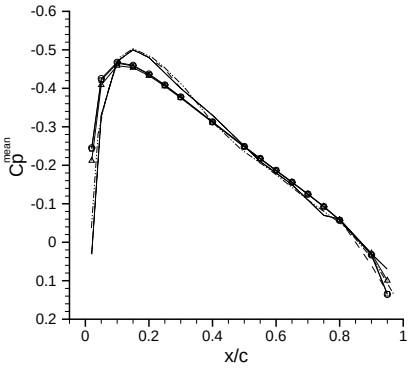

(a) The mean value of the pressure coefficient c_p.

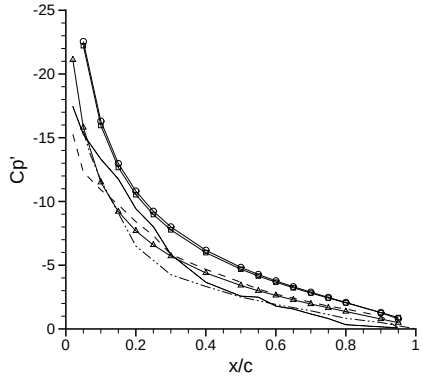

(b) Real part c'_p.

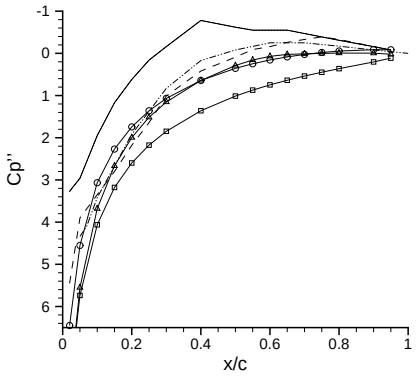

(c) Imaginary part c''_p.

Figure 8: (a) The mean value of the pressure coefficient c_p, (b) real part c'_p and (c) imaginary part c''_p for $\varphi_0 = 3°$: —Δ—, computed values (DTSM scheme, ALE method); —○—, computed values (LWR scheme, ALE method); —□—, computed values (LWR scheme, SDT); – – –, Triebstein theory; ···, Triebstein experiment [7]; – · · –, Benetka experiment [8].

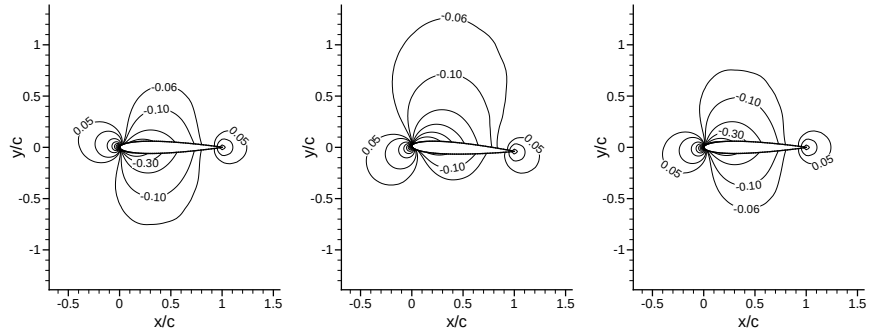

(a) $\varphi = 0°$ (b) $\varphi = 3°$ (c) $\varphi = 0°$

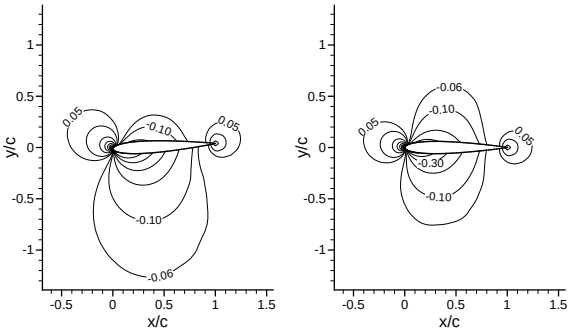

(d) $\varphi = -3°$ (e) $\varphi = 0°$

Figure 9: Pressure coefficient isolines around the vibrating profile NACA 0012, data computed using DTSM scheme.

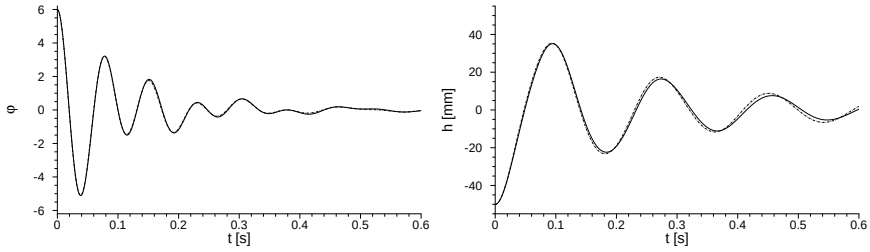

Figure 10: Angle of rotation φ and vertical displacement h, initial conditions $h(0) = -50$ mm, $\dot{h}(0) = 0$, $\varphi(0) = 6°$, $\dot{\varphi}(0) = 0$, $(u_\infty, v_\infty) = (15, 0)$ m/s: ——, data computed using LWR scheme; – · –, data computed using DTSM scheme. Linearized equations of profile motion considered.

The simulation of fluid-structure interaction as a function of time is presented in Figure 10. The left, resp. right panel shows the angle of rotation φ, resp. the vertical displacement h in dependence on time for inflow velocity $(u_\infty, v_\infty) = (15, 0)$ m/s. Results obtained using the LWR scheme (in ALE formulation) and the DTSM scheme for initial conditions $h(0) = -50$ mm, $\dot{h}(0) = 0$, $\varphi(0) = 6°$, $\dot{\varphi}(0) = 0$ are compared.

Figure 11 presents frequency spectrum analysis carried out using Fast Fourier Transform applied to the history of angle of rotation φ and vertical displacement h for far-field flow velocity vector $(u_\infty, v_\infty) = (15, 0)$ m/s computed with the use of LWR scheme in ALE formulation. One can see two dominant frequencies. The lower one refers to the vertical translation of the profile and the higher one to the rotation of the profile around the elastic axis.

7.4 Viscous Flow Simulations

Rather preliminary numerical results of viscous flows over the profile NACA 0012 are presented. The computational domain is outlined in Figure 5. The kinematic viscosity is $\nu = 1.5 \times 10^{-5}$ m/s^2. All simulations performed consider the upstream velocity vector $(u_\infty, v_\infty) = (10, 0)$ m/s, which corresponds to the Reynolds number $Re = 2 \times 10^5$. The C-type mesh is accordingly refined at the viscous wall to be able to capture the viscous layer.

Figure 12 refers to numerical simulation of flow induced vibrations of the profile with two degrees of freedom. Input parameters used by the simulation

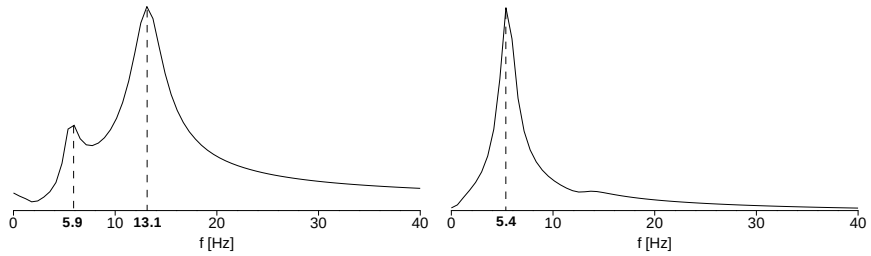

Figure 11: Frequency spectrum analysis of angle of rotation φ (left) and vertical displacement h (right) history in time, $(u_\infty, v_\infty) = (15, 0)$ m/s, computed using LWR scheme and linearized equations of profile motion.

are the same as in the numerical examples presented in Section 7.3. Initial conditions are $h(0) = -10$ mm, $\dot{h}(0) = 0$, $\varphi(0) = 3°$, $\dot{\varphi}(0) = 0$.

Conclusions

A finite volume solver of two-dimensional incompressible flows with aeroelastic effects was developed and implemented. The main progress was done in inviscid flow simulations. Nevertheless, promising preliminary results of numerical solutions of laminar viscous flows considering aeroelastic effects were also achieved. The aeroelastic effects are represented by flow induced vibrations of a profile with two degrees of freedom in this work.

Explicit numerical schemes for solving steady state flows are presented. These schemes in conjunction with the artificial compressibility method were proven to be applied to steady state simulations performed within this work. It is demonstrated by the presented numerical results and their comparison with experimental data. The experimental and computed data are in a good agreement. Convergence history diagrams confirm the robustness of the methods used.

A numerical analysis of four slip wall boundary condition realizations was made. It consisted in exploiting Bernoulli's principle and comparing numerical results obtained for all four alternatives.

Two approaches were considered for numerical solution of unsteady governing equations - an artificial compressibility approach and a dual-time stepping method. To deal with deformations of the computational domain due to the

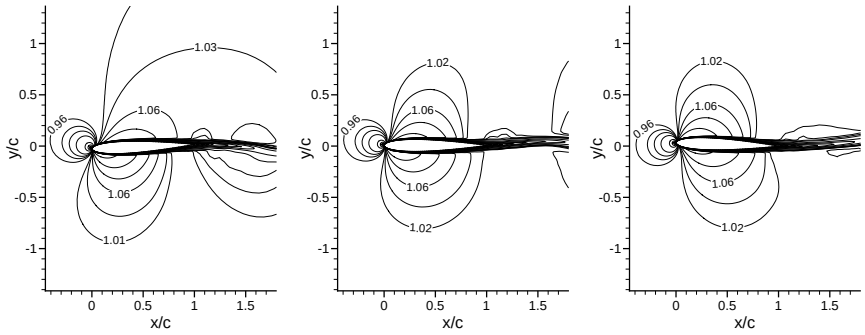

(a) $\varphi = -2.50°$, $h = -2.78$ mm

(b) $\varphi = 0.01°$, $h = 1.95$ mm

(c) $\varphi = 1.93°$, $h = 5.79$ mm

Figure 12: Isolines of velocity value field around the vibrating profile NACA 0012, $(u_\infty, v_\infty) = (10, 0)$ m/s, data computed using DTSM scheme.

profile motion, two methods were applied - the small disturbance theory and the arbitrary Lagrangian-Eulerian method. First, numerical results concerning prescribed periodic oscillations of the profile are presented. Computed data are compared with experimental and theoretical ones. The best fitting results are given by the dual-time stepping scheme in arbitrary Lagrangian-Eulerian formulation. Second, numerical solutions of freely oscillating profile with two degrees of freedom are shown. The governing equations of the profile motion were considered in both linearized and nonlinear form. The results are compared with NASTRAN flutter analysis data. Good agreement was achieved. The robustness of the dual-time stepping method is illustrated by the convergence history graphs in dual time.

The last section of the work is devoted to rather preliminary steady state and unsteady numerical simulations of viscous flow past a profile. However, from the qualitative point of view they are promising for continuation in development of the viscous flow solver.

The future steps intended are to continue in an improvement of the viscous flow solver for unsteady simulations with aeroelastic effects and to extend the methods for three-dimensional problems.

Název práce: **Numerické řešení nestlačitelného proudění s dynamickými a aeroelastickými účinky**

Anotace

Práce se zabývá numerickým řešením nestlačitelného proudění s uvažováním interakce proudící tekutiny a kmitajícího profilu se dvěma stupni volnosti.

První část je věnována systému Eulerových a Navier-Stokesových rovnic představujících matematické modely dvourozměrného nevazkého resp. vazkého nestlačitelného proudění a dále okrajovým podmínkám aplikovaným na hranicích oblasti řešení. Jelikož jsou v numerických výpočtech užity bezrozměrné formy výše zmíněných matematických modelů, je v této části též uveden převod rozměrového na bezrozměrný tvar těchto rovnic.

V druhé části jsou popsány aplikované numerické metody. Stručně je shrnut princip metody konečných objemů, je představena metoda umělé stlačitelnosti užitá při řešení stacionárního nevazkého a vazkého nestlačitelného proudění a jsou prezentována explicitní numerická schémata implementovaná autorem. Pro lineární skalární rovnici advekce s konstantními koeficienty ve dvou prostorových dimenzích je provedena analýza stability, jež vede na podmínku omezující časový krok výpočtu. Tato podmínka je v mírně změněné podobě využita v implementovaných algoritmech. Dále jsou uvedeny numerické metody pro řešení nestacionárního nestlačitelného proudění, konkrétně přístup umělou stlačitelností a metoda s duálním časem. Pro zacházení s deformacemi výpočetní oblasti způsobenými pohybem profilu je aplikována jednak metoda malých poruch a jednak arbitrary Lagrangian-Eulerian metoda. Podrobně jsou popsána schémata pro numerické řešení nestacionárního proudění a numerické realizace užitých okrajových podmínek. Jsou zde také odvozeny rovnice popisující pohyb profilu a je popsáno jejich numerické řešení.

Poslední část se věnuje výsledkům numerických simulací jak pro nevazké tak pro laminární vazké proudění. Jsou zde prezentovány výsledky stacionárních i nestacionárních výpočtů, z nichž některé jsou srovnány s experimentálními daty.

References

[1] E. H. Dowell, R. Clark, D. Cox, H. C. Curtiss Jr., J. W. Edwards, K. C. Hall, D. A. Peters, R. Scanlan, E. Simiu, F. Sisto, T. W. Strganac, A Modern Course in Aeroelasticity, 4th Edition, Kluwer Academic Publishers, 2004.

[2] M. P. Païdoussis, Fluid-Structure Interactions, Vol. 1, Academic Press, 1998.

[3] F. Axisa, J. Antunes, Fluid-Structure Interaction, 1st Edition, Vol. 3, Elsevier, 2007.

[4] J. Luchta, Sborník charakteristik profilů křídel, Technical report 1669/55, VTA AZ, Brno, (in Czech) (1955).

[5] J. Benetka, Měření kmitajícího profilu v různě vysokých měřících prostorech, Technical report Z-2610/81, Aeronautical Research and Test Institute, Prague, Letňany, (in Czech) (1981).

[6] R. C. Dixon, High Reynolds number investigation of an Onera model of the NACA 0012 airfoil section, NAE-LTR-HA 5X5/0069, Ottawa, Canada (1975).

[7] H. Triebstein, Steady and unsteady transonic pressure distributions on NACA0012, Journal of Aircraft 23 (3) (1986) 213–219.

[8] J. Benetka, J. Kladrubský, R. Valenta, Measurement of NACA 0012 profile in a slotted measurement section, Technical report R-2909/98, Aeronautical Research and Test Institute, Prague, Letňany, (in Czech) (1998).

[9] J. Fűrst, Numerical solution of compressible flows using TVD and ENO finite volume methods, habilitation, Faculty of Mechanical Engineering, Czech Technical University in Prague (2004).

[10] L. D. Laundau, E. M. Lifshitz (Eds.), Fluid mechanics, Pergamon Press, Oxford, 1987.

[11] J. Blazek, Computational fluid dynamics: principles and applications, 1st Edition, Elsevier, 2001.

[12] R. J. LeVeque, Finite volume methods for hyperbolic problems, 1st Edition, Cambridge University Press, Cambridge, 2002.

[13] D. Krőner, Numerical schemes for conservation laws, Wiley, 1997.

[14] D. L. Brown, R. Cortez, M. L. Minion, Accurate projection methods for the incompressible Navier-Stokes equations, Journal of Computational Physics 168 (2001) 464–499.

[15] J. P. Jessee, W. A. Fiveland, A cell vertex algorithm for the incompressible Navier-Stokes equations on non-orthogonal grids, International Journal for Numerical Methods in Fluids 23 (1996) 271–293.

[16] C. Kiris, K. Dochan, Numerical solution of incompressible Navier-Stokes equations using a fractional-step approach, Computers & Fluids 30 (2001) 829–851.

[17] A. J. Chorin, A numerical method for solving incompressible viscous flow problems, Journal of Computational Physics 2 (1) (1967) 12–26.

[18] C. T. Chan, K. Anastasiou, Solution of incompressible flows with or without a free surface using the finite volume method on unstructured triangular meshes, International Journal for Numerical Methods in Fluids 29 (1999) 35–57.

[19] P. Louda, Numerické řešení dvourozměrného a třírozměrného turbulentního impaktního proudění, Ph.D. thesis, Fakulta strojní, České vysoké učení technické v Praze (2002).

[20] E. Turkel, Algorithms for the Euler and Navier-Stokes equations for supercomputers, ICASE Report 85-11, Institute for Computer Applications in Science and Engineering, Hampton, VA (1985).

[21] E. Turkel, Review of preconditioning for the compressible fluid dynamic equations, CFD review (1998).

[22] K. Kozel, J. Fűrst, Numerické metody řešení problémů proudění I, 1st Edition, Vydavatelství ČVUT, Praha, 2001.

[23] A. Jameson, W. Schmidt, E. Turkel, Numerical solution of the Euler equations by finite volume methods using Runge-Kutta time-stepping schemes, in: AIAA Paper 1981-1259, Palo Alto, California, 1981.

[24] L. Beneš, Numerické řešení proudění v mezní vrstvě atmosféry, Ph.D. thesis, Fakulta strojní, České vysoké učení technické v Praze (2000).

[25] K. Kozel, Numerické řešení nevazkého stacionárního transonického proudění, Ph.D. thesis, Fakulta strojní, České vysoké učení technické v Praze (1990).

[26] A. Jameson, Essential elements of computational algorithms for aerodynamic analysis and design, ICASE Report 97-68, Institute for Computer Applications in Science and Engineering, Hampton, VA (1997).

[27] R. J. LeVeque, Numerical methods for conservation laws, Birkhäuser Verlag, Basel, 1990.

[28] K. Kozel, R. Dvořák, Matematické modelování v aerodynamice, 1st Edition, Vydavatelství ČVUT, Praha, 1996.

[29] J. Fořt, K. Kozel, P. Louda, J. Fűrst, Numerické metody řešení problémů proudění III, 1st Edition, Vydavatelství ČVUT, Praha, 2004.

[30] A. L. Gaitonde, A dual-time method for two-dimensional unsteady incompreessible flow calculations, International Journal for Numerical Methods in Engineering 41 (1998) 1153–1166.

[31] A. Arnone, M. Marconcini, R. Pacciani, On the use of dual time stepping in unsteady turbomachinery flow calculations, in: ERCOFTAC Bulletin, no. 42, 1999, pp. 37–42.

[32] A. Arnone, M. S. Liou, A. L. Povinelli, Multigrid time-accurate integration of Navier-Stokes equations, in: AIAA Paper 93-3361, 1993.

[33] M. Feistauer, J. Felcman, I. Straškraba, Mathematical and computational methods for compressible flow, Claredon Press, Oxford, 2003.

[34] T. Fanion, M.-A. Fernández, P. Le Tallec, Deriving adequate formulations for fluid-structure interaction problems: from ale to transpiration, Rapport de recherche no 3879, Institut National de Recherche en Informatique et en Automatique, Le Chesnay Cedex, France (Feb. 2000).

[35] M. Lesoinne, C. Farhat, Geometric conservation laws for flow problems with moving boundaries and deformable meshes, and their impact on aeroelastic computations, Computer Methods in Applied Mechanics and Engineering 134 (1996) 71–90.

[36] L. Formaggia, F. Nobile, Stability analysis of second-order time accurate schemes for ALE-FEM, Computer Methods in Applied Mechanics and Engineering 193 (2004) 4097–4116.

[37] T. Nomura, T. J. R. Hughes, An arbitrary Lagrangian-Eulerian finite element method for interaction of fluid and a rigid body, Computer Methods in Applied Mechanics and Engineering 95 (1992) 115–138.

[38] M. Feistauer, Mathematical methods in fluid dynamics, Longman Scientific and Technical, Harlow, 1993.

[39] A. Quarteroni, Simulation of fluid and structure interaction, Lecture Notes, European Mathematical Society EURO SUMMER SCHOOL, Prague (Aug. 2001).

[40] B. Koobus, C. Farhat, Second-order time-accurate and geometrically conservative implicit schemes for flow computations on unstructured dynamic meshes, Computer Methods in Applied Mechanics and Engineering 170 (1999) 103–129.

[41] K. Kozel, J. Polášek, M. Vavřincová, Numerical solution of transonic flow through a cascade with slender profiles, in: Proc. of VI. Int. Conf. on Numerical Methods in Fluid Dynamics, SAN Moskva, 1979.

[42] K. Kozel, J. Polášek, M. Vavřincová, Mathematische Methoden zur Berechnung den Transonischen Umstrőmung von dűnnen Profilen, in: Teubner Texte zur Mathematik, Equadiff 5, Leipzig, 1982.

[43] K. Kozel, J. Polášek, M. Vavřincová, Numerical solution of transonic shear flows past thin bodies, in: Proc. of 8. Int. Conf. in Fluid Dynamics, Aachen, 1982.

[44] K. Kozel, M. Vavřincová, Finite difference solution of low-frequency unsteady subsonic and transonic flows past thin profiles, in: Numerical Methods and Applications, Sofia, 1984.

[45] K. Kozel, M. Vavřincová, Numerical solution of unsteady transonic flows past thin profiles, in: Lecture Notes in Physics, no. 217, Springer Verlag, 1985.

[46] Z. J. Wang, Y. Sun, Curvature-based wall boundary condition for the Euler equations on unstructured grids, AIAA Journal 41 (1) (2003) 27–33.

[47] R. P. Feynman, R. B. Leighton, M. Sands, Feynmanovy přednášky z fyziky, 1st Edition, Vol. 3, Fragment, 2001.

[48] J. Horáček, Nonlinear formulation of oscillations of a profile for aero-hydroelastic computations, in: Dobiáš (Ed.), Dynamics of Machines, Prague, 2003, pp. 51–56.

[49] P. Sváček, M. Feistauer, J. Horáček, Numerical simulation of flow induced airfoil vibrations with large amplitudes, Journal of Fluids and Structures 23 (3) (2007) 391–411.

[50] E. H. Dowell, A modern course in aeroelasticity, Kluwer Academic Publisher, Dodrecht, 1995.

[51] E. Vitásek, Numerické metody, 1st Edition, SNTL - Nakladatelství technické lite-ratury, n. p., Praha, 1987.

[52] A. Shmilovich, D. A. Caughey, Grid generation for wing-tail-fuselage configurations, Journal of Aircraft 22 (6) (1985) 467–472.

[53] R. E. Sheldahl, P. C. Klimas, Aerodynamic characteristics of seven airfoil sections through 180 degrees angle of attack for use in aerodynamic analysis of vertical axis wind turbines, SAND80-2114, Sandia National Laboratories, Albuquerque, New Mexico (Mar. 1981).

[54] L. Dubcová, M. Feistauer, J. Horáček, P. Sváček, Numerická simulace interakce leteckého profilu a turbulentního proudění, Research report Z 1388/06, Institute of Thermomechanics, AS CR, Prague, (in Czech) (2007).

[55] J. Čečrdle, J. Maleček, Verification FEM model of an aircraft construction with two and three degrees of freedom, Technical report R-3418/02, Aeronautical Research and Test Institute, Prague, Letňany, (in Czech) (2002).

[56] T. J. Chung, Computational fluid dynamics, 1st Edition, Cambridge University Press, Cambridge, 2002.

[57] J. Kozánek, D. Scopel, Rayleigh's field in dynamics, in: Proc. of Colloquium Dynamics of Machines 2000, Institute of Thermomechanics, AS CR, Prague, 2000, pp. 109–116.

[58] C. D. Meyer, Matrix Analysis and Applied Linear Algebra, SIAM, 2000.

Publications related to the dissertation thesis

[1] R. Honzátko, M. Janda, K. Kozel, Kompozitní schéma užité k numerickému řešení stacionárního proudění popsaného systémem Eulerových rovnic, in: P. Jonáš, V. Uruba (Eds.), Proceedings of Fluid Dynamics '99, Institute of Thermomechanics AS CR, 1999, pp. 111–114.

[2] R. Honzátko, M. Janda, K. Kozel, Numerické řešení 2D stacionárního a nestacionárního proudění užitím kompozitního schématu (Numerical solution of 2D steady and unsteady flows using composite schemes), in: Proceedings of Fluid Mechanics 2000, Institute of Thermomechanics AS CR, 2000, pp. 27–30.

[3] R. Honzátko, M. Janda, K. Kozel, Numerical solution of 2D steady and unsteady flows using composite schemes, in: Proceedings of Algoritmy 2000, Vysoké Tatry - Podbanské, Slovakia, 2000, pp. 68–74.

[4] R. Honzátko, J. Horáček, K. Kozel, Numerické řešení nestlačitelného nevazkého obtékání mříže s uvažováním dynamických účinků (Numerical solution of incompressible inviscid flow through a cascade considering dynamical effects), in: Proceedings of Fluid Mechanics 2001, Institute of Thermomechanics AS CR, 2001, pp. 57–60.

[5] R. Honzátko, J. Horáček, K. Kozel, Numerické řešení obtékání oscilujícího profilu v kanálu (Numerical solution of flow past an oscillating profile in a channel), in: Proceedings of Fluid Mechanics 2002, Institute of Thermomechanics AS CR, 2002, pp. 33–36.

[6] R. Honzátko, J. Horáček, K. Kozel, Numerical solution of flow over a profile considering dynamical and aeroelastic effects, in: Proceedings of Algoritmy 2002, Vysoké Tatry - Podbanské, Slovakia, 2002, pp. 187–194.

[7] R. Honzátko, J. Horáček, K. Kozel, Numerical solution of unsteady flow over a profile in a channel, in: Sborník semináře Programy a algoritmy numerické matematiky 11, Matematický ústav AV ČR, Dolní Maxov, 2002, pp. 65–72.

[8] R. Honzátko, J. Horáček, K. Kozel, Numerical solution of some 2D incompressible flow using dynamical effects, in: Topical Problems of Fluid Mechanics 2003, Institute of Thermomechanics AS CR, 2003, pp. 29–34.

[9] R. Honzátko, J. Horáček, K. Kozel, Steady and unsteady flow over a profile in a channel, in: P. Jonáš, V. Uruba (Eds.), Proceedings of Fluid Dynamics 2003, Institute of Thermomechanics AS CR, 2003, pp. 31–34.

[10] R. Honzátko, J. Horáček, K. Kozel, Dynamical and aeroelastic effects in a numerical solution of flow through a cascade and over a profile, in: M. Kočandrlová, V. Kelar (Eds.), Proceedings of the International Conference Mathematical and Computer Modeling in Science and Engineering, Prague, 2003, pp. 152–156.

[11] R. Honzátko, J. Horáček, K. Kozel, Numerical solution of steady and unsteady flow over given profile in a channel, in: I. I. Zolotarev CSc. (Ed.), Proceedings Interaction and Feedbacks '2003, no. 10, Institute of Thermomechanics AS CR, Prague, 2003, pp. 43–50.

[12] R. Honzátko, J. Horáček, K. Kozel, Numerical solution of flow through a cascade and over a profile with dynamical and aeroelastic effects, in: PAMM (Proceedings in Applied Mathematics and Mechanics), Vol. 3, Wiley-VCH Verlag, 2003, pp. 282–283, www.gamm-proceedings.com.

[13] R. Honzátko, K. Kozel, J. Horáček, Numerical solution of flow through a cascade and over a profile with dynamical and aeroelastic effects, in: E. de Langre, F. Axisa (Eds.), Proc. of the 8th International Conference on Flow-Induced Vibration, FIV2004, Paris, 2004, pp. 377–382.

[14] R. Honzátko, J. Horáček, K. Kozel, Numerical solution of flow over a vibrating airfoil, in: Zolotarev (Ed.), Proceedings Interaction and Feedbacks '2004, no. 11, Institute of Thermomechanics AS CR, Prague, 2004, pp. 23–30.

[15] R. Honzátko, K. Kozel, J. Horáček, Flow over a profile in a channel with dynamical effects, in: PAMM (Proceedings in Applied Mathematics and Mechanics), Vol. 4, Wiley-VCH Verlag, 2004, pp. 322–323, www.gamm-proceedings.com.

[16] R. Honzátko, J. Horáček, K. Kozel, Numerical solution of inviscid incompressible flow in a channel with dynamical effects, in: Programs and Algorithms of Numerical Mathematics 12, Matematický ústav AV ČR, Dolní Maxov, 2004, pp. 76–81.

[17] J. Fűrst, R. Honzátko, J. Horáček, K. Kozel, Flow over a given profile in a channel with dynamical effects, in: M. Beneš, J. Mikyška, T. Oberhuber (Eds.), Proceedings of Czech-Japanese Seminar in Applied Mathematics 2004, Dept. of Mathematics, Faculty of Nuclear Sciences and Physical Engineering, Czech Technical University in Prague, Prague, 2005, pp. 63–72.

[18] R. Honzátko, K. Kozel, J. Horáček, Numerical solution of steady and unsteady flow over a vibrating airfoil in a channel, in: PAMM (Proceedings in Applied Mathematics and Mechanics), Vol. 5, Wiley-VCH Verlag, 2005, pp. 465–466, www.gamm-proceedings.com.

[19] R. Honzátko, K. Kozel, J. Horáček, Numerical solution of inviscid incompressible flow over a vibrating profile, in: COE Lecture Note Series, Vol. 3, Kyushu University, Japan, 2006, pp. 26–32.

[20] R. Honzátko, K. Kozel, J. Horáček, Numerical solution of 2D incompressible flow over a vibrating airfoil, in: CMFF'06 Conference Proceedings, Budapest University of Technology and Economics, Department of Fluid Mechanics, Budapest, 2006, pp. 233–240.

[21] R. Honzátko, J. Horáček, K. Kozel, Numerical solution of flow over a vibrating profile with two degrees of freedom, in: Topical Problems of Fluid Mechanics 2007, Ústav termomechaniky AV ČR, Prague, 2007, pp. 61–64.